Synergistic effects of Cu_2O-decorated CeO_2 on photocatalytic CO_2 reduction: Surface Lewis acid/base and oxygen defect

Yu Pu[a,b], Yidan Luo[a,b], Xiaoqian Wei[a,b], Jingfang Sun[b], Lulu Li[a,b,c], Weixin Zou[a,b,c], Lin Dong[a,b,c,*]

[a] Key Laboratory of Mesoscopic Chemistry of MOE, School of Chemistry and Chemical Engineering, Nanjing University, Nanjing, 210093, PR China
[b] Jiangsu Key Laboratory of Vehicle Emissions Control, Center of Modern Analysis, Nanjing University, Nanjing, 210093, PR China
[c] State Key Laboratory of Pollution Control and Resource Reuse, School of the Environment, Nanjing University, Nanjing, 210093, PR China

ARTICLE INFO

ABSTRACT

Ceria (CeO_2) with abundant oxygen defects, surface alkalinity, low cost effectiveness and admirable redox ability could be used in the photoreduction of CO_2. However, little attention has been paid to the interaction of reactant CO_2 molecules on CeO_2–based photocatalysts. In this work, Cu_2O nanoparticles were applied to the modification of the properties of Lewis acid/base, surface oxygen defect content and visible light adsorption of CeO_2, and the adsorption/activation abilities of CO_2 reactant on Cu_2O/CeO_2 and CeO_2 photocatalysts were investigated in comparison. The photocatalytic performance showed that Cu_2O/CeO_2 had better activity than CeO_2. And the loading of Cu_2O resulted in more oxygen defects and Ce^{3+} species, which was helpful for available visible light adsorption and higher charge-separation efficiency. Furthermore, CO_2-TPD, CO_2-adsorption DRIFTS and in-situ ESR results demonstrated that the synergistic effects of Cu_2O/CeO_2 were beneficial for more generated carboxylate and $^{\cdot}CO_2{}^{-}$ radicals, instead of carbonate species which promoted CO_2 reduction to CO.

1. Introduction

With the development of industrialization, the considerable environmental issues have been generated during the fossil fuel combustion [1], leading to a urgent search for sustainable energy and controlling carbon emissions. In general, carbon dioxide (CO_2) is one of the greenhouse gases, although it increases global temperature, CO_2 could fulfill partial energy needs in demand. Therefore, the utilization of CO_2 as resources is exceedingly important for both the energy and environment problems. Artificial photosynthesis is of significance, because atmospheric CO_2 levels decrease and value added chemicals such as CO, methane, formaldehyde, formic acid, etc. could be simultaneously produced during the photo-reduction of CO_2 [2,3]. On the basis of that, a great number of efforts have been taken to develop highly-efficient photocatalysts for CO_2 reduction.

Ceria (CeO_2), as a n-type semiconductor, has attracted great attention in photocatalysis for its abundant oxygen defects, low cost effectiveness and admirable redox ability, but there are still some disadvantages, such as fast recombination of electron-hole, less visible light adsorption, low quantum efficiency, which have bad influences on the application [4,5]. Therefore, many strategies has been used to improve the performance of CeO_2 photocatalyst. Primo et al. found that the loading of Au could enhance the visible light photocatalytic activity

[6]. Tian et al. synthesized CeO_2/TiO_2 nanobelt heterostructures and proposed that the efficient capture of reactants on CeO_2 surface was one of the important factors to improve the photocatalytic performance [7]. Recently, it has been reported that CeO_2-based materials also could be applied in the field of CO_2 photoreduction [8,9]. Generally, for the reaction process of CO_2 photo-reduction, the capture of CO_2 reactants, available visible light adsorption and fast photo-generated charge transfer are indispensable for photocatalytic activity [10–13]. Based on these, the control of surface acid/base and oxygen defects of CeO_2-based catalysts is of great importance to CO_2 photoreduction.

Cuprous oxide (Cu_2O) is a common p-type semiconductor and was widely used as a co-catalyst in photocatalysis, due to narrow band gap. Wang et al. proposed that the assembly of p-type Cu_2O nanoparticles could produce a large number of p–n junction heterostructures on the surface of $BiVO_4$. The p–n junction heterostructures enhanced the speed of charge transfer in photocatalysts and successfully increased the visible-light photocatalytic activity [14]. A series of Cu_2O-loaded Zn-Cr layered double hydroxides were prepared by Jiang et al. and the loaded Cu_2O nanoparticles probably acted as effective electron traps, promoting charge separation and providing active sites for CO_2 reduction [15]. Furthermore, Cu_2O is a promising material to modify CeO_2. Hu et al. prepared Cu_2O-CeO_2 and evaluated the photocatalytic efficiency by degradation of Acid Orange 7 in water [16]. Chae et al. synthesized

* Corresponding author.
E-mail address: donglin@nju.edu.cn (L. Dong).

CeO_2-Cu_2O composite nanofibers for degradation of MB [17]. It was found that the photocatalytic performance of the prepared sample was much higher than that of pure CeO_2, for the reason that p-type Cu_2O and n-type CeO_2 form the p–n heterojunction. CeO_2/Cu_2O heterojunction was also efficient for photoelectrochemical water splitting [18]. On the basis of the related reports, these Cu_2O/CeO_2 catalysts were mainly focused on the photocatalytic pollution degradation and water splitting, little attention was paid on the photocatalytic CO_2 reduction, especially, the effects of Cu_2O on the acid/base and oxygen defects of CeO_2 and the synergistic interactions between Cu_2O and CeO_2 were worthy of investigation.

Therefore, in this work, Cu_2O/CeO_2 nanoparticles were synthesized and the synergistic interactions between Cu_2O and CeO_2 on CO_2 photoreduction were investigated in detail. The result of activity suggested that Cu_2O/CeO_2 had more CO evolution than that of pure CeO_2. XPS, Raman and low temperature ESR spectra showed that the Cu_2O loading led to more oxygen defects and Ce^{3+}/Ce^{4+} ratio, which promoted visible light absorption and charge separation efficiency of Cu_2O/CeO_2. Furthermore, the interactions of CO_2 reactant on Cu_2O/CeO_2 and CeO_2 photocatalysts were studied by CO_2-TPD, CO_2-adsorption diffuse infrared Fourier transform (DRIFT) and in-situ ESR characterizations. The schematic illustration of the synergistic effects of Cu_2O/CeO_2 on the CO_2 photoreduction was proposed. This study showed that the consideration of surface reaction is necessary to photocatalytic CO_2 reduction.

2. Experimental

2.1. Catalyst preparation

The CeO_2 support was obtained through the cerium nitrate hexahydrate calcination in air at 450 °C for 4 h. Then the mixture of Cu$(Ac)_2$ and CeO_2 were ultrasonic for 0.5 h and stirred in a fume hood for 24 h to remove water. The obtained solids were calcined in a tube furnace in N_2 at 450 °C for 4 h. The nominal weight ratio of Cu to Ce was 2 wt%. The obtained Cu_2O/CeO_2 sample was denoted as CuCe. The CeO_2 support was denoted as CeO_2. 1% CuCe and 5% CuCe samples were synthesized as above with different Cu/Ce ratios. Cu_2O powders and the CeO_2 support were physically mixed with a ratio of 2 wt% and the obtained sample was denoted as 2% CuCe-physical mixture.

2.2. Catalyst characterization

Transmission electron microscopy (TEM) characterization was taken on JEM-2100 instrument by an acceleration voltage of 200 kV. The sample was crushed and dispersed in ethanol, and the obtained suspension was dropped and dried on copper grids with carbon film. The crystal structures of CuCe and CeO_2 were determined by X-ray diffraction (XRD) on Philips X'Pert Pro diffractometer under Ni-filtered Cu Kα radiation (λ = 0.15418 nm). Brunauer–Emmet–Teller (BET) surface areas were measured by nitrogen adsorption at 77 K on a Micrometrics ASAP-2020 adsorption apparatus. Before each adsorption measurement, approximate 0.1 g sample was degassed in a N_2/He mixture at 300 °C for 3 h. The X-ray tube was operated at 40 kV and 40 mA. X-ray photoelectron spectroscopy (XPS) analysis was determined by PHI 5000 Versa Probe high performance electron spectrometer, on monochromatic Al Kα radiation (1486.6 eV), the sample was outgassed at room temperature in a UHV chamber ($< 5 \times 10^{-7}$ Pa). The charging effect on sample was compensated by binding energies referenced to 284.6 eV of C 1 s peak. This reference provided binding energies with an error within ± 0.1 eV. The FT-IR spectra were collected from 400 to 4000 cm^{-1} on Nicolet 5700 FT-IR spectrometer at the spectral resolution of 4 cm^{-1}. UV–vis diffuse reflectance spectroscopy (UV–vis DRS) was recorded in the range of 200–700 nm with the reference of $BaSO_4$ by a Shimadzu UV-2401 spectrophotometer. The electron spin resonance (ESR) signal was examined at 77 K on ESR JES

FA200 (JEOL) spectrometer, and in-situ ESR under the irradiation of Xenon lamp were used the trapping agents PBN (N-tert-butyl-2-phenylnitrone) and DMPO (5,5-dimethyl-1-pyrroline N-oxide) and obtained the signal of CO_2^- free radical. Raman spectra were obtained on a LABRAM-HR Confocal Laser with He–Cd lasers (325 nm) excitation source. Photoluminescence (PL) spectra were determined on an F-7000 fluorescence spectrophotometer (Hitachi, Tokyo, Japan). The wave length of the excitation light was 325 nm. The experiments were carried out in the solid state. The slit in all measurements was 1.5 nm. CO_2-TPD experiments were carried out on a multifunction chemisorption analyzer (Tianjin Pengxiang, China) with a quartz U-tube reactor and detected by a TCD. Each sample (100 mg) was heated under ultra-high purity N_2 flow (30 mL/min) up to 200 °C at 10 °C/min for 1 h and then it was cooled to room temperature. After pretreatment, CO_2 flow (30 mL/min) passed through the catalyst bed for 30 min, subsequently the sample was flushed by N_2 flow (30 mL/min) for 60 min. Then, the TPD analysis was performed under N_2 flow (30 mL/min) by heating the sample at a rate of 10 °C/min up to 750 °C. In situ diffuse infrared Fourier transform (in situ DRIFT) spectra were recorded in the frequency range of 1200–4000 cm^{-1} at a spectral resolution of 4 cm^{-1} (number of scans: 32) on a Nicolet 5700 FT-IR spectrometer equipped with a highly sensitive mercury cadmium telluride detector cooled by liquid N_2. The DRIFT cell (Harrick) was equipped with a KBr window and a heater that allowed samples to be heated to 400 °C. The catalyst powders placed on a sample holder were carefully flattened to enhance the IR reflection. The samples were purged with a N_2 stream at 150 °C to eliminate physisorbed water and other impurities. After pretreatment, CO_2 flow passed through when it was cooled to room temperature until saturation adsorption. Then N_2 flow under room temperature was used to eliminate physisorbed CO_2 and the DRIFTS spectra were measured afterwards.

2.3. Catalytic performances measurement

The CO_2 photoreduction was carried out under 300 W Xe lamp irradiation, which was the only heat throughout the whole experiment, in a 50 mL Teflon-lined autoclave. The photocatalyst (50 mg) was dispersed in 5 mL of water and high purity of CO_2 was added up to 4 bar. The suspension was stirred for 30 min and then irradiated for 8 h with a full spectrum or visible light. The generated CO was measured by a gas chromatograph. The recycle experiment was performed as followed: every cycle was carried out for 8 h. During the interruption of each cycle, the used catalyst was washed with distilled water for 3 times, and finally dried in an oven at 80 °C.

3. Results and discussion

3.1. Structure of catalysts

The TEM and high resolution (HR)TEM characterizations of CuCe catalyst were carried out and the results were shown in Fig. S1. There were no Cu clusters observed on the surface of CuCe catalyst. The HRTEM results suggested that the obtained CeO_2 catalysts were dominantly exposed {111} facets. The phase structures of CeO_2 and CuCe samples were determined by XRD characterization. From Fig. S2, all peaks were assigned to the cubic fluorite-type CeO_2 (PDF-ICDD 34-0394), and no other signals attributed to Cu species were observed, which indicated that the copper species are highly dispersed on the surface or the low copper loading is beyond the limitation of XRD detection [19,20]. The results of the BET surface area of CeO_2 and CuCe samples were displayed in Table S1, respectively. It was shown that CuCe and CeO_2 had similar surface areas. On the basis of XRD and BET surface area, it could be deduced that the loading of copper species had no obvious influences on the textural properties of CeO_2 catalyst.

The valence states of copper species on CeO_2 catalyst was of great importance to the photocatalytic performance. Therefore, the XPS
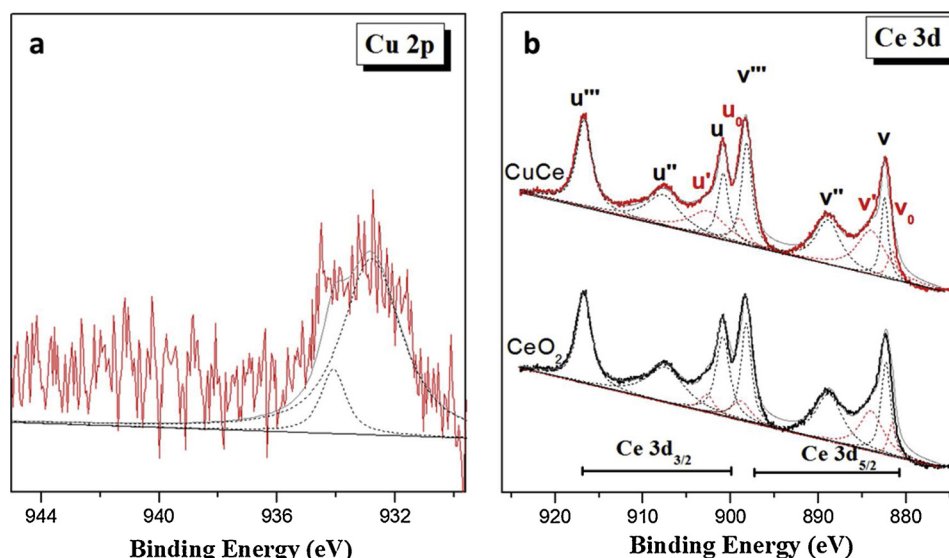
Fig. 1. XPS spectra of (a) Cu 2p and (b) Ce 3d of CuCe and CeO_2 samples.

characterization was used to study the status of elementary oxidation states and the results were displayed in Fig. 1. According to the literatures, in Cu 2p XPS spectra, the peak with binding energy of 934.4 eV was ascribed to Cu^{2+} while the peak at 932.1 eV was assigned to Cu^+ species. [10] In Fig. 1a, the broad peak could be fitted into two peaks attributed to Cu^+ and Cu^{2+} species, respectively. It was observed that most of the copper species on CeO_2 surface was in the form of Cu^+, and the presence of little Cu^{2+} species was resulted from inevitable incorporation of Cu^+ into the surface lattice of CeO_2 and the generation of redox equilibrium ($Cu^+ + Ce^{4+} \leftrightarrow Cu^{2+} + Ce^{3+}$). At the same time, the surface Ce species were further analyzed to confirm. As shown in Fig. 1b, Ce 3d spectra consisted of two multiplets assigned to $3d_{3/2}$ and $3d_{5/2}$, respectively. The band was fitted into eight peaks, which were labelled as u' and v' ascribed to Ce^{3+} and the other six peaks were Ce^{4+} species, respectively. [21–23] As listed in Table S1, the ratios of Ce^{3+}/Ce^{4+} were calculated, in the order of CuCe (0.47) > CeO_2 (0.26). On the basis of that, the Cu_2O species was loaded on CeO_2 support, which was applied in the following investigations in comparison with CeO_2, in order to explore the effects of Cu_2O on the photocatalytic CO_2 reduction.

3.2. Photocatalytic performance

The photocatalytic CO_2 reduction was operated in the presence of water vapor under the irradiation of full spectrum. The photocatalytic performances of CO_2 reduction on 2% CuCe and CeO_2 samples were
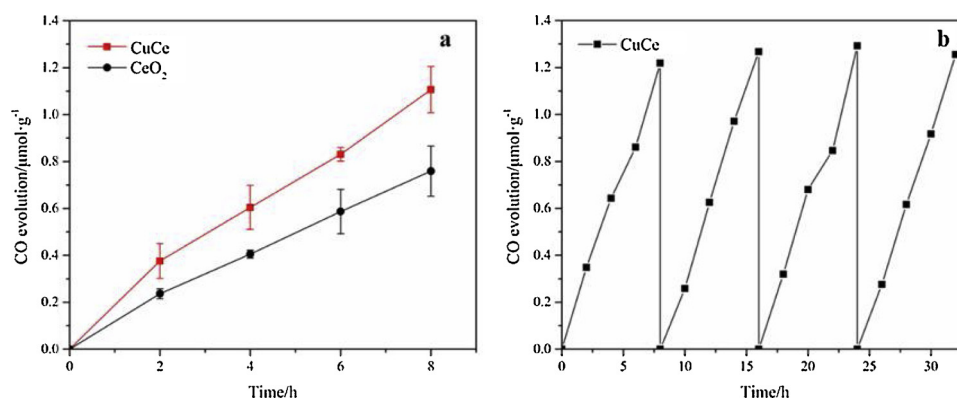
evaluated and the results were shown in Fig. 2a. Compared to the pure CeO_2 sample, 2% CuCe had better photoactivity of CO evolution for irradiation 8 h. However, no hydrocarbon was detected by a gas chromatograph. The photocatalytic stability was further determined and the recycling test of 2% CuCe was shown in Fig. 2b. After four cycles, no obvious decreased CO evolution was observed, suggesting that the CuCe catalyst exhibited excellent photostability during reaction time. In addition, the photocatalytic performances of CuCe samples with different Cu/Ce ratios (1%, 2%, and 5%) were compared and shown in Fig. S3. The 2% CuCe catalyst exhibited better CO evolution than 1% and 5% CuCe samples. Furthermore, the blank experiments were carried out as following processes, respectively, in order to confirm the accuracy of the results. (1) Stirring 8 h in dark with the catalyst, CO_2 and H_2O; (2) stirring 8 h under light irradiation with CO_2 and H_2O, and no catalyst was present; (3) stirring 8 h under light irradiation with the catalyst and H_2O, and no CO_2 was present. From the above three processes, there were no obvious CO evolution, respectively (Fig. S4). On the basis of that, the obtained results of photocatalytic CO_2 reduction on CuCe and CeO_2 samples were considered reasonable, and 2% CuCe (denoted as CuCe) catalyst was chosen to investigate the synergistic effects between Cu_2O and CeO_2 on CO_2 reduction reaction as followed.

3.3. Optical property

To identify the optical adsorption properties of CuCe and CeO_2 samples, the UV–vis DRS was characterized. From Fig. 3a, the CuCe
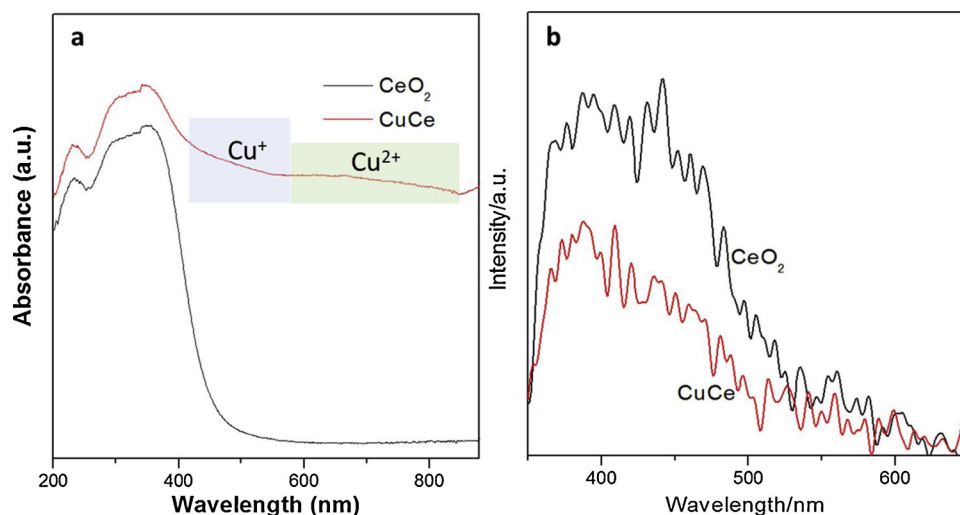

Fig. 2. (a) CO production of CuCe and CeO_2 samples under illumination and (b) the recycling rest of CO production of CuCe.

Fig. 3. (a) UV–vis absorption spectra and (b) PL spectra of CuCe and CeO$_2$ samples.

sample showed a stronger absorption in the visible light range. It can be noted that a weak band at around 450 nm was assigned to the formation of Cu$^+$ and the broad and weak band in the region of 600–800 nm could be attributed to the $2E_g \rightarrow 2T_{2g}$ spin-allowed d–d transition of Cu^{2+} ions, [24,25] which were consistent with the XRD results of copper species. Therefore, the loading of Cu$_2$O on CeO$_2$ improved visible light adsorption, leading to more charges and holes generation under light irradiation.

The PL spectra was used to investigate the interface charge carrier transfer and the photo induced electron–hole pair separation efficiency [26]. Furthermore, the PL characterization was determined to compare the recombination of photo-generated charge-hole of CuCe and CeO$_2$ samples. As observed in Fig. 3b, CuCe and CeO$_2$ samples displayed similar emission peaks at about 400 nm, which was resulted from the charge transfer transition from Ce 4f to O 2p level [27]. When Cu$_2$O was loaded on CeO$_2$, the intensity of this emission peak decreased. It demonstrated that the separation efficiency of the photo induced electron–hole pair was highly improved on CuCe sample.

3.4. Oxygen defects

In general, the oxygen defects were indispensable for photocatalysis in many aspects. Therefore, we employed Raman, XPS, and ESR characterizations to study the oxygen defect property affected by Cu$_2$O loaded on CeO$_2$. In the Raman spectra (Fig. 4a), there was an obvious peak at ca. 460 cm^{-1}, which was assigned to the symmetric stretching vibrations mode F$_{2g}$ of CeO$_2$, and a shoulder peak at ca. 600 cm^{-1} attributed to the defect-induced band was observed [28,29].

Furthermore, a broad band (1150–1230 cm^{-1}) was ascribed to O−O stretching on surface superoxide complexes (O$_2$-), resulted from the oxygen defect [30]. And the peak intensities of I$_{600}$ + I$_{1150}$/I$_{460}$ on CuCe and CeO$_2$ samples were calculated in Table S1, respectively, in the order of CuCe (0.41) > CeO$_2$ (0.04). It could be found that the band intensity of oxygen defects was increased on CuCe sample, and thus Cu$_2$O loaded on CeO$_2$ was beneficial for the generation of oxygen defects. The XPS spectra of O 1s on CuCe and CeO$_2$ catalysts further confirmed, and the results exhibited in Fig. 4b. The peaks at 529.0 and 531.5 eV were ascribed to CeO$_2$ lattice oxygen and chemisorbed oxygen species on surface, respectively [31]. Compared the peak positions of lattice oxygen on CuCe and CeO$_2$ samples, it was found that the position of lattice oxygen on CuCe shifted to higher binding energy than that of CeO$_2$, which indicated that the introduce of Cu$_2$O made the electronic density of lattice oxygen decreased, possibly resulted from the formation of oxygen defect on CuCe.

In addition, ESR characterization at 77 K was employed and the results were shown in Fig. 4c. In the low field region on the spectra, four hyperfine splitting features for paramagnetic Cu^{2+} ions appeared, and in the high field region, the signal peak on CuCe were broader related to CuO, which might be resulted from the heterogeneity of chemical environment and defect structures [32]. Meanwhile, the signal of g = 1.956 recognized as Ce^{3+} species was observed on CuCe sample, which could indicate that oxygen detects were formed [33]. On the basis of the above XPS, ESR and Raman characterizations, it could be concluded that when Cu$_2$O was loaded on CeO$_2$, more oxygen defects were generated than that of CeO$_2$.
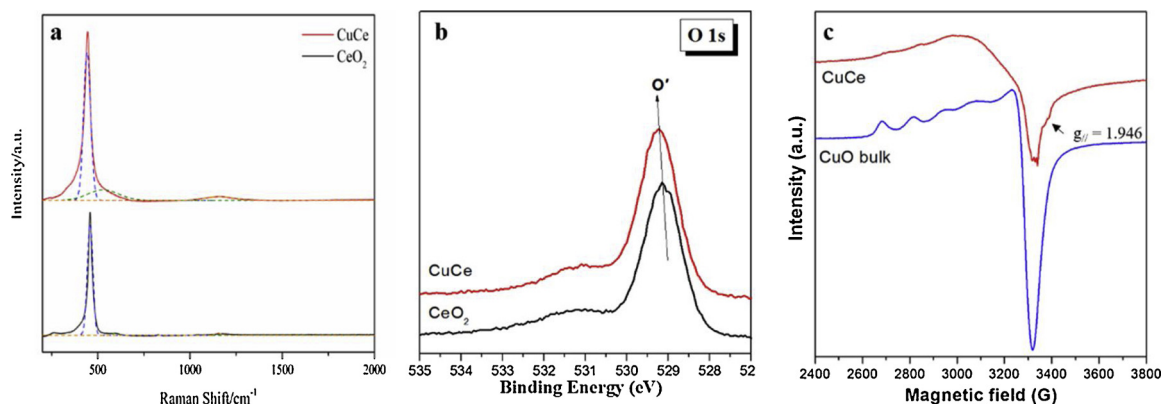

Fig. 4. (a) Raman spectra of CuCe and CeO$_2$ samples; (b) O 1s XPS spectra of CuCe and CeO$_2$; and (c) ESR results at 77 K of CuCe and CuO samples.
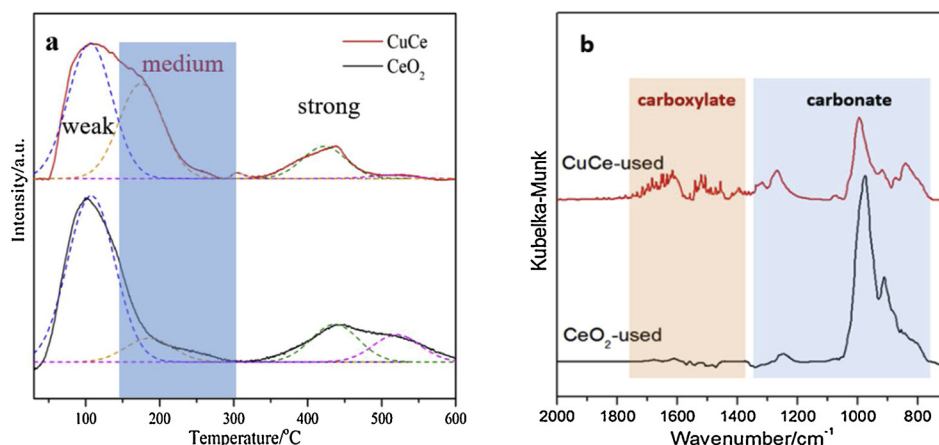
Fig. 5. (a) CO_2-TPD spectra of CuCe and CeO_2 samples; and (b) CO_2 adsorption DRIFTS of the used CuCe and CeO_2 samples.

3.5. CO₂ adsorption and activation

As we all known, surface reaction included of the reactant adsorption on the catalyst surface was of great importance in photocatalysis, and thus CO_2-TPD characterization was used to investigate the interaction of CO_2 reactant on CuCe and CeO_2 catalysts in comparison. The CO_2-TPD results were shown in Fig. 5a. The desorption of CO_2 adsorbed on samples showed three major peaks, i.e., molecularly adsorbed CO_2 (75–180 °C), HCO_3^- or HCO_2^- (180–350 °C), bidentate carbonates (b-CO_3^{2-}) (380–550 °C), and monodentate carbonates (m-CO_3^{2-}) (550–760 °C), which were attributed to weak, medium, and strong basic sites of catalysts, respectively [34,35]. The molecularly adsorbed CO_2 at lower temperature indicated the weak interaction between CO_2 reactant and sample [20]; at higher temperature, the interactions became stronger. For the HCO_3^- or HCO_2^- species, it came from the reaction of CO_2 and hydroxyls on surface, and the m-CO_3^{2-} and b-CO_3^{2-} species were generated from CO_2 molecule combined with oxygen atoms or both oxygen and metal atom of catalysts [20]. In Table S1, the ratio of medium base to the whole base on CuCe and CeO_2 samples were calculated, i.e., 0.36 and 0.09, respectively. On the basis of that, it was suggested that when Cu_2O was loaded on CeO_2, the surface property of acid/base was changed, and more medium basic sites were generated than that of pure CeO_2. It was reported that for Cu_2O and CeO_2 polyhedron nanoparticles, the Cu_2O (111) and CeO_2 (111) were the major exposed crystal planes, on which CO_2 adsorbed states were different, i.e., C atom of CO_2 bind with Cu on Cu_2O (111) to form carboxylate (HCO_2^-), while O atom of CO_2 bind with Ce on CeO_2 (111) forming carbonate (CO_3^{2-}) [36]. In CO_2-TPD results, the generated HCO_2^- and CO_3^{2-} suggested medium and strong adsorption of CO_2 on catalysts, respectively. Generally, too weak or strong adsorption of reactant molecules on the catalyst was not beneficial for the surface reaction. On the basis of that, it was proposed that the CeO_2 modification by Cu_2O had a positive influence on CO_2 adsorption, which would be helpful for the activation of CO_2 reactant, and then photoreduction to CO.

Furthermore, the used CuCe and CeO_2 catalysts after photocatalytic reaction were determined, and suggested that CO_2 reactants were easier to activation on CuCe than that of CeO_2 catalyst. The results of XRD and FT-IR of the used CuCe and CeO_2 catalysts were shown in Fig. S5. In Fig. S5a, a weak peak at 20° attributed to carbonate species [37] was observed on the used CuCe sample, while no phenomenon was found on the used CeO_2 catalyst. Similarly, the FT-IR spectra also demonstrated the result. In the used CuCe sample, the bands at ca. 1230 and 1130 cm^{-1} were appeared, which were related to the carbonate species [38–40]. To further confirm that the formed carbonate species on the used CuCe catalyst was helpful for the photocatalytic CO_2 reduction, the CO_2 adsorption DRIFTS were measured on the used catalysts and the corresponding results were displayed in Fig. 5b. According to

literatures, there were some adsorbed species, i.e., carboxylate (1684, 1500 and 1274 cm^{-1}), HCO_3- (1600, 1417, 1398, and 1217 cm^{-1}), b-CO_3^{2-} (1278 cm^{-1}) and m-CO_3^{2-} (1460 and 1310 cm^{-1}) [38–40]. Compared the used CuCe and CeO_2, it was proposed that more carboxylate species were formed on the used CuCe, while CO_3^{2-} species was easily generated on the used CeO_2. It was reported that the generation of carboxylate species indicated that CO_2 reactant was easier to be activated [39]. Therefore, the introduce of Cu_2O on CeO_2 promoted the adsorption and activation of CO_2 reactant, which played an important role in the CO_2 photoreduction.

In order to identify the advantageous effect of Cu_2O on the photocatalytic CO_2 reduction, the in-situ ESR under light illumination were used to analyze the radicals on CuCe and CeO_2 samples in comparison. From Fig. 6, three significant peaks could be clearly observed in the ESR spectra when using PBN as the spin trapper. According to literatures [41,42], the ESR signal was attributed to the generated $\cdot CO_2^-$ radicals in the reaction. It was found that after Cu_2O loading, the signal intensity of the $\cdot CO_2^-$ radicals was increased, suggesting that the Cu_2O loading on CeO_2 was beneficial for CO_2 activation and reduction under light irradiation.
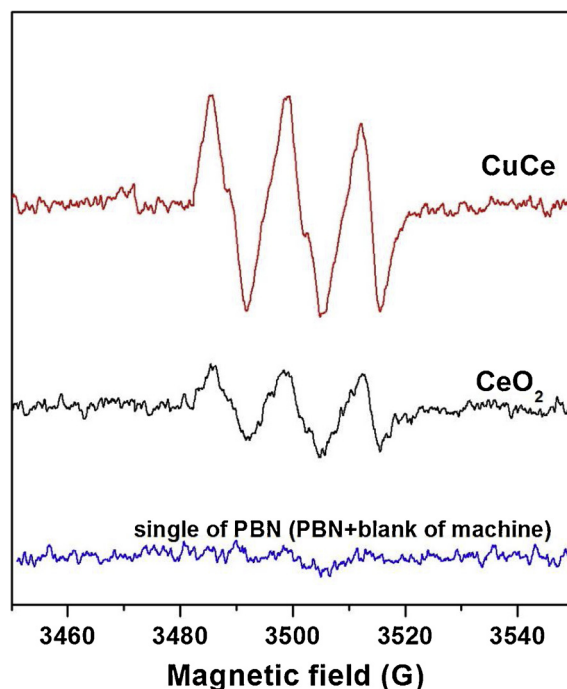

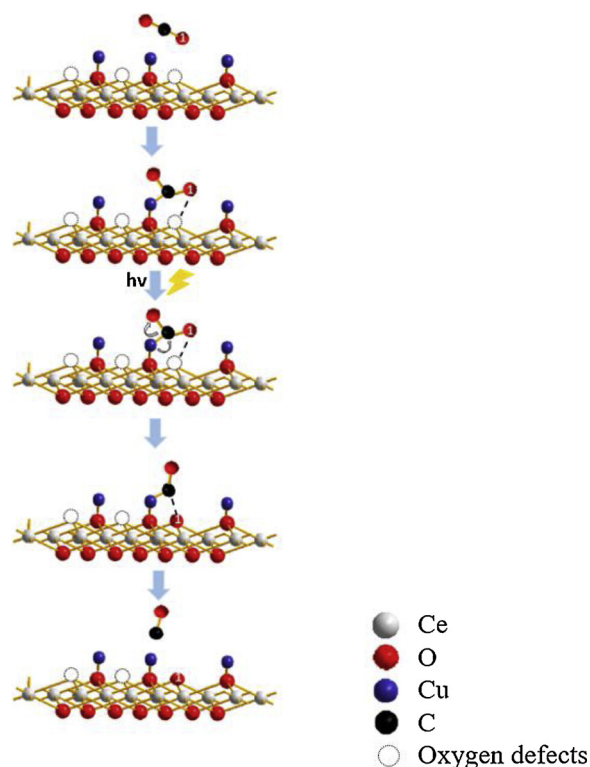**Fig. 6.** The profiles of ESR signal of the radicals in the reaction.

Fig. 7. The possible reaction mechanism of the CO_2 photoreduction on CeO_2 and CeCe samples.

3.6. Mechanism

On the basis of the results of UV–vis DRS, PL, Raman, XPS, low-temperature ESR, CO_2-TPD, in-situ ESR, it could be proposed that when Cu_2O was decorated on CeO_2, the property of surface acid/base and oxygen defects of the photocatalyst were modified, leading to the available visible light adsorption, fast photo-generated charge transfer, more surface medium basic sites, the adsorption and activation of CO_2 reactant, and the improved photocatalytic performance of CO_2 reduction.

The schematic illustration was employed to describe the synergistic effects of CuCe catalyst on CO_2 photoreduction, and the reaction mechanism was shown in Fig. 7. The above-mentioned synergistic interactions for the CO_2 reduction to CO mainly came from the Lewis base site (Cu_2O) and oxygen defect (CeO_2). Firstly, the CO_2 molecule was adsorbed on the Cu atoms of Cu_2O via the d electron of Cu to C [36], and the adsorbed carboxylate CO_2^- species was formed on Cu sites; secondly, under light irradiation, the photo-generated electron transferred from Cu to C–O bond of carboxylate, and the O atom of carboxylate interacted with the oxygen vacancy (O_v) on CeO_2 surface, and then the O atom transferred to O_v; Finally, the above interaction promoted the break of C–O bond of the adsorbed carboxylate species, and thus CO molecule was generated. Therefore, the role of Cu_2O was of great significance, leading to the improved surface Lewis acid-basic sites and oxygen defects of CeO_2, and the above synergistic effects were beneficial for the enhanced CO_2 photoreduction.

4. Conclusions

CeO_2 was modified by Cu_2O and the effects of Cu_2O on the photocatalytic CO_2 reduction by CuCe sample were investigated. The CuCe sample has enhanced CO_2 photoreduction performance than pure CeO_2, because the introduce of Cu_2O resulted in the stronger visible light absorption, higher electron-hole pair separation efficiency, more oxygen defects, Lewis base sites, and active radical $\cdot CO_2^-$ species.

Furthermore, the synergistic interaction of Cu_2O and CeO_2 was facilitated to the adsorption/activation of CO_2 molecules and CO evolution.

Acknowledgements

Appendix A. Supplementary data

Supplementary material related to this article can be found, in the online version, at doi:https://doi.org/10.1016/j.apcatb.2019.04.093.

References

[1] S. Chu, A. Majumdar, Opportunities and challenges for a sustainable energy future, Nature 488 (7411) (2012) 294.

[2] M. Ulman, A. Tinnemans, A. Mackor, B. Aurian-Blajeni, M. Halmann, Photoreduction of carbon dioxide to formic acid, formaldehyde, methanol, acetaldehyde and ethanol using aqueous suspensions of strontium titanate with transition metal additives, Int. J. Sol. Energy 1 (3) (1982) 213–222.

[3] Y. Wang, B. Li, C. Zhang, L. Cui, S. Kang, X. Li, L. Zhou, Ordered mesoporous CeO2-TiO2 composites: highly efficient photocatalysts for the reduction of CO2 with H2O under simulated solar irradiation, Appl. Catal. B: Environ. 130 (2013) 277–284.

[4] M.M. Khan, S.A. Ansari, D. Pradhan, D.H. Han, J. Lee, M.H. Cho, Defect-induced band gap narrowed CeO2 nanostructures for visible light activities, Ind. Eng. Chem. Res. 53 (23) (2014) 9754–9763.

[5] S. Xie, Z. Wang, F. Cheng, P. Zhang, W. Mai, Y. Tong, Ceria and ceria-based nanostructured materials for photoenergy applications, Nano Energy 34 (2017) 313–337.

[6] A. Primo, T. Marino, A. Corma, R. Molinari, H. Garcia, Efficient visible-light photocatalytic water splitting by minute amounts of gold supported on nanoparticulate CeO2 obtained by a biopolymer templating method, J. Am. Chem. Soc. 133 (18) (2011) 6930–6933.

[7] J. Tian, Y. Sang, Z. Zhao, W. Zhou, D. Wang, X. Kang, H. Liu, J. Wang, S. Chen, H. Cai, Enhanced photocatalytic performances of CeO2/TiO2 nanobelt heterostructures, Small 9 (22) (2013) 3864–3872.

[8] H. Abdullah, M.R. Khan, M. Pudukudy, Z. Yaakob, N.A. Ismail, CeO2-TiO2 as a visible light active catalyst for the photoreduction of CO2 to methanol, J. Rare Earths 33 (11) (2015) 1155–1161.

[9] Y. Wang, J. Zhao, T. Wang, Y. Li, X. Li, J. Yin, C. Wang, CO2 photoreduction with H2O vapor on highly dispersed CeO2/TiO2 catalysts: surface species and their reactivity, J. Catal. 337 (2016) 293–302.

[10] W. Zou, L. Zhang, L. Liu, X. Wang, J. Sun, S. Wu, Y. Deng, C. Tang, F. Gao, L. Dong, Engineering the Cu2O–reduced graphene oxide interface to enhance photocatalytic degradation of organic pollutants under visible light, Appl. Catal. B: Environ. 181 (2016) 495–503.

[11] X. Bai, L. Wang, R. Zong, Y. Lv, Y. Sun, Y. Zhu, Performance enhancement of ZnO photocatalyst via synergic effect of surface oxygen defect and graphene hybridization, Langmuir 29 (9) (2013) 3097–3105.

[12] Z.F. Huang, J. Song, L. Pan, F. Lv, Q. Wang, J.-J. Zou, X. Zhang, L. Wang, Mesoporous W 18 O 49 hollow spheres as highly active photocatalysts, Chem. Commun. 50 (75) (2014) 10959–10962.

[13] F. Lei, Y. Sun, K. Liu, S. Gao, L. Liang, B. Pan, Y. Xie, Oxygen vacancies confined in ultrathin indium oxide porous sheets for promoted visible-light water splitting, J. Am. Chem. Soc. 136 (19) (2014) 6826–6829.

[14] W. Wang, X. Huang, S. Wu, Y. Zhou, L. Wang, H. Shi, Y. Liang, B. Zou, Preparation of p–n junction Cu2O/BiVO4 heterogeneous nanostructures with enhanced visible-light photocatalytic activity, Appl. Catal. B: Environ. 134 (2013) 293–301.

[15] H. Jiang, K.-i. Katsumata, J. Hong, A. Yamaguchi, K. Nakata, C. Terashima, N. Matsushita, M. Miyauchi, A. Fujishima, Photocatalytic reduction of CO2 on Cu2O-loaded Zn-Cr layered double hydroxides, Appl. Catal. B: Environ. 224 (2018) 783–790.

[16] S. Hu, F. Zhou, L. Wang, J. Zhang, Preparation of Cu2O/CeO2 heterojunction photocatalyst for the degradation of acid orange 7 under visible light irradiation, Catal. Commun. 12 (9) (2011) 794–797.

[17] B.W. Chae, T. Amna, M.S. Hassan, S.S. Al-Deyab, M.-S. Khil, CeO2-Cu2O composite nanofibers: synthesis, characterization photocatalytic and electrochemical application, Adv. Powder Technol. 28 (1) (2017) 230–235.

[18] D. Sharma, V.R. Satsangi, R. Shrivastav, U.V. Waghmare, S. Dass, Understanding the photoelectrochemical properties of nanostructured CeO2/Cu2O heterojunction photoanode for efficient photoelectrochemical water splitting, Int. J. Hydrogen Energy 41 (41) (2016) 18339–18350.

[19] L. Li, W. Tan, X. Wei, Z. Fan, A. Liu, K. Guo, K. Ma, S. Yu, C. Ge, C. Tang, Mo doping as an effective strategy to boost low temperature NH3-SCR performance of CeO2/TiO2 catalysts, Catal. Commun. 114 (2018) 10–14.

[20] X. Yao, T. Kong, L. Chen, S. Ding, F. Yang, L. Dong, Enhanced low-temperature NH3-SCR performance of MnOx/CeO2 catalysts by optimal solvent effect, Appl. Surf. Sci. 420 (2017) 407–415.

[21] L. Qi, Q. Yu, Y. Dai, C. Tang, L. Liu, H. Zhang, F. Gao, L. Dong, Y. Chen, Influence of

cerium precursors on the structure and reducibility of mesoporous CuO-CeO2 catalysts for CO oxidation, Appl. Catal. B: Environ. 119 (2012) 308–320.

[22] S. Watanabe, X. Ma, C. Song, Characterization of structural and surface properties of nanocrystalline TiO2− CeO2 mixed oxides by XRD, XPS, TPR, and TPD, J. Phys. Chem. C 113 (32) (2009) 14249–14257.

[23] Z. Wu, R. Jin, Y. Liu, H. Wang, Ceria modified MnOx/TiO2 as a superior catalyst for NO reduction with NH3 at low-temperature, Catal. Commun. 9 (13) (2008) 2217–2220.

[24] P. Gao, F. Li, F. Xiao, N. Zhao, N. Sun, W. Wei, L. Zhong, Y. Sun, Preparation and activity of Cu/Zn/Al/Zr catalysts via hydrotalcite-containing precursors for methanol synthesis from CO 2 hydrogenation, Catal. Sci. Technol. 2 (7) (2012) 1447–1454.

[25] Y. Xiong, L. Li, L. Zhang, Y. Cao, S. Yu, C. Tang, L. Dong, Migration of copper species in Ce x Cu 1− x O 2 catalyst driven by thermal treatment and the effect on CO oxidation, Phys. Chem. Chem. Phys. 19 (32) (2017) 21840–21847.

[26] Y. Luo, J. Wang, S. Yu, Y. Cao, K. Ma, Y. Pu, W. Zou, C. Tang, F. Gao, L. Dong, Nonmetal element doped gC 3 N 4 with enhanced H 2 evolution under visible light irradiation, J. Mater. Res. 33 (9) (2018) 1268–1278.

[27] B. Choudhury, P. Chetri, A. Choudhury, Annealing temperature and oxygen-vacancy-dependent variation of lattice strain, band gap and luminescence properties of CeO2 nanoparticles, J. Exp. Nanosci. 10 (2) (2015) 103–114.

[28] S. Chang, M. Li, Q. Hua, L. Zhang, Y. Ma, B. Ye, W. Huang, Shape-dependent interplay between oxygen vacancies and Ag–CeO2 interaction in Ag/CeO2 catalysts and their influence on the catalytic activity, J. Catal. 293 (2012) 195–204.

[29] M. Lohrenscheit, C. Hess, Direct evidence for the participation of oxygen vacancies in the oxidation of carbon monoxide over ceria-supported gold catalysts by using operando Raman spectroscopy, ChemCatChem 8 (3) (2016) 523–526.

[30] S. Liu, X. Wu, W. Liu, W. Chen, R. Ran, M. Li, D. Weng, Soot oxidation over CeO2 and Ag/CeO2: factors determining the catalyst activity and stability during reaction, J. Catal. 337 (2016) 188–198.

[31] M. Piumetti, S. Bensaid, N. Russo, D. Fino, Nanostructured ceria-based catalysts for soot combustion: investigations on the surface sensitivity, Appl. Catal. B: Environ.

165 (2015) 742–751.

[32] Y. Cao, L. Liu, F. Gao, L. Dong, Y. Chen, Understanding the effect of CuO dispersion state on the activity of CuO modified Ce0. 7Zr0. 3O2 for NO removal, Appl. Surf. Sci. 403 (2017) 347–355.

[33] K. Zhao, J. Qi, H. Yin, Z. Wang, S. Zhao, X. Ma, J. Wan, L. Chang, Y. Gao, R. Yu, Efficient water oxidation under visible light by tuning surface defects on ceria nanorods, J. Mater. Chem. A 3 (41) (2015) 20465–20470.

[34] J. Zhao, Y. Wang, Y. Li, X. Yue, C. Wang, Phase-dependent enhancement for CO 2 photocatalytic reduction over CeO 2/TiO 2 catalysts, Catal. Sci. Technol. 6 (22) (2016) 7967–7975.

[35] K. Pokrovski, K.T. Jung, A.T. Bell, Investigation of CO and CO2 adsorption on tetragonal and monoclinic zirconia, Langmuir 17 (14) (2001) 4297–4303.

[36] S. Chen, T. Cao, Y. Gao, D. Li, F. Xiong, W. Huang, Probing surface structures of CeO2, TiO2, and Cu2O nanocrystals with CO and CO2 chemisorption, J. Phys. Chem. C 120 (38) (2016) 21472–21485.

[37] S. Wang, G.M. Lu, Role of CeO2 in Ni/CeO2–Al2O3 catalysts for carbon dioxide reforming of methane, Appl. Catal. B: Environ. 19 (3-4) (1998) 267–277.

[38] D. Forney, M.E. Jacox, W.E. Thompson, Infrared spectra of trans-HOCO, HCOOH + , and HCO 2− trapped in solid neon, J. Chem. Phys. 119 (20) (2003) 10814–10823.

[39] L. Liu, Y. Jiang, H. Zhao, J. Chen, J. Cheng, Y. Kang, Y. Li, Engineering coexposed {001} and {101} facets in oxygen-deficient TiO2 nanocrystals for enhanced CO2 photoreduction under visible light, ACS Catal. 6 (2) (2016) 1097–1108.

[40] Y. Yoshida, Y. Arai, S. Kado, K. Kunimori, K. Tomishige, Direct synthesis of organic carbonates from the reaction of CO2 with methanol and ethanol over CeO2 catalysts, Catal. Today 115 (1-4) (2006) 95–101.

[41] Q. Zhang, C.-F. Lin, B.-Y. Chen, T. Ouyang, C.-T. Chang, Deciphering visible light photoreductive conversion of CO2 to formic acid and methanol using waste prepared material, Environ. Sci. Technol. 49 (4) (2015) 2405–2417.

[42] Q. Zhang, F. Liu, J.M. Hong, C.-F. Lin, C.-T. Chang, Efficiency, mechanism and kinetics research of CO2 photo reduction by graphene-TiO2 under visible light, J. Nanosci. Nanotechnol. 17 (7) (2017) 5073–5080.